# Journal of Materials Chemistry B

Accepted Manuscript






ROYAL SOCIETY OF CHEMISTRY

www.rsc.org/materialsB

Journal Name

ARTICLE

# Detection of fibronectin conformational changes in the extracellular matrix of live cells using plasmonic nanoplates

Received 00th January 20xx,
Accepted 00th January 20xx

DOI: 10.1039/x0xx00000x

www.rsc.org/

Margaret E. Brennan-Fournet,[a]* Miriam Huerta [a], Yi Zhang [a], George Malliaras[a] and Roisin M. Owens [a]

Protein conformational changes are detected both in vitro and for the first time in the presence of living cells using versatile plasmonic nanoplates. Au-edge-coated triangular silver nanoplates (AuTSNP) exhibit some of the highest refractive index sensitivity values recorded to date and exhibit a strong spectral response to surface biomolecular interactions. Large spectral shifts of over 30 nm distinguish between pH induced compact and extended conformations of the ubiquitous extracellular matrix protein Fibronectin (Fn). Conformational transition of Fn from compact to extended is accompanied by a red spectral shift of 27 nm while a corresponding blue spectral shift of 25 nm accompanies the reverse conformational transition. Cleavage of Fn by cathepsin B, which plays an important role in cellular functions and in cancer metastasis is characterised by a blue spectral shift with detection in serum using a straightforward no-wash assay demonstrated. Spectral monitoring of nanoplates decorated with Fn and incubated with MDCK II cells shows extensive shifts of 156 nm and cellular morphological re-arrangement as Fn uncoils from a compact format to from fibrils within the extra cellular matrix.

## Introduction

Conformational changes in protein structures play a prominent role in the control of regulatory functions in cells. Protein misfolding, aggregation or degradation can result in the onset of several diseases, including Alzheimer's, Parkinson's, type II diabetes and cancer.[1-4] Techniques and tools to characterize structural variations in proteins, both in the presence of cells and tissues are required to progress our knowledge of protein based diseases towards the development of new treatments and therapies. A host of methods are available to measure real-time protein structural activity and folding in vitro including, Raman spectroscopy, FTIR and circular dichorism.[5] NMR can also provide detailed mapping of protein secondary structure via isotope labeling, however, intense computational power requirements limit its application for real-time measurements.[6] The crowded cell matrix, with its variable local viscosity and microstructure is known to modulate protein folding compared to isolated studies done in solution.[7] Measurement of protein conformational dynamics in the cellular environment is essential to compare with and build upon the extensive information gained from previous studies. The techniques used in solution, however, are generally greatly hindered by the high level of background noise within the complex cellular environment.[7] Mass spectrometry has been used to provide a snapshot of protein structure within cells.8 Adaptations to NMR has enabled studies of protein structure inside of living cells, although with long data collection times.[9] Fluorescence methods[7], in particular fluorescence resonance energy transfer (FRET)[10,11] and total internal reflection fluorescence (TIRF)[12] can provide details of in-cell conformational changes, but require the protein to be pre-labelled and the use of optical microscopy.

Fibronectin (Fn) is a critical protein within the extracellular matrix (ECM) with important functions for cellular activity and studies on this protein would benefit greatly from new techniques for dynamic monitoring of protein folding. This ubiquitous extracellular protein undergoes distinctive conformational changes that control its extensive biological activity.[13-15] Fn is a 440 kDa dimer glycoprotein which plays an important role in cellular adhesion and migration processes, embryogenesis, wound healing, blood coagulation and is implicated in metastasis, tumour development and carcinoma.[16-20] Changes measured in Fn expression and increased Fn degradation are associated with the promotion of tumour growth and survival. The quaternary Fn structure in physiological buffer (pH 7.4) has a compact, folded conformation with dimensions of 16 nm – 24 nm.[13] At lower pH, Fn unfolds with the extended dimer length estimated to be 130 nm.[19] Within cells Fn binds cell receptors called integrins and assembles into high molecular weight fibrils.[17,18] The intra and extracelllar degradation of many proteins including Fn is mediated by cysteine proteases such as Cathepsin B (CTSB). Located in lysosomes, CTSB has its optimum activity in an

[a] Ecole Nationale Supérieure des Mines, CMP-EMSE, Centre Microélectronique de Provence, 880, route de Mimet, 13541 Gardanne, France.

† Footnotes relating to the title and/or authors should appear here.

Electronic Supplementary Information (ESI) available: [details of any supplementary information available should be included here]. See DOI: 10.1039/x0xx00000x

acidic pH but still shows some activity at neutral pH.[21] CTSB expression is increased in malignant tumours and premalignant lesions where it is secreted and localises at the cell surface.[4,22] Degradation of the extracellular matrix (including Fn cleavage by CTSB) is associated with the early steps in the development of cancer, assisting tumour cell detachment and metastasis.[23,24] A straightforward serum assay for CTSB would provide a useful diagnostic tool, given the correlation with invasiveness, particularly in breast and prostate tumours.[25]

An in vitro study of un-labelled protein conformational transitions has recently been reported using surface confined Ag nanotriangles, wherein shifts of less than 1 nm were reported for the opening and closing conformational translation of calmodulin, a calcium binding intercellular protein.[26] The nanoplates used in this work were solution phase Au-edge-coated triangular silver nanoplates (AuTSNP) which exhibit some of the highest refractive index sensitivity values recorded to date.[27,28] These nanoplates have high aspect ratios which serve to increase the sensing range over thicker nanostructures.[26,29,30] However, nanostructures which are not immobilised on a substrate are advantageous, as they are in phase with the biomolecular target, support recognition kinetics and are accessible for measurements with live cells.[27] Here we demonstrate a label-free method for detection of protein con-formational changes both in solution and for the first time in the presence of live cells, using highly sensitive local surface plasmon resonant (LSPR) AuTSNP nano-plates. Systematic shifts in the spectra of LSPR nanostructures can be induced upon the interaction of molecules which generate a change in the refractive index local to the nanostructure surface.[31] This spectral selectivity arises from the collective oscillation of the conduction electrons in response to impinging light and generates enhanced electromagnetic fields at the nanostructure surface. This localised sensitivity eliminates the need for protein labelling making LSPR nanostructures highly favourable for protein conformational sensing.[26]

Using the LSPR spectral shifts of AuTSNP nanoplates we first distinguish between compact and extended con-formations of Fn. The transition of Fn from extended to compact conformation is readily tracked in real-time. Changes in Fn size due to cleavage by CTSB are also shown. A straightforward versatile serum assay for CTSB is demonstrated, based on the LSPR detection of Fn cleavage. FRET experiments in the presence of cells have previously shown the transformation of Fn in compact formation at physiological pH, to form extensive fibrils due to cell integrin binding processes.[32] Here, straight-forward LSPR spectral shifts are used to monitor the progression of compact Fn diffusely bound to cells to form Fn fibril matrices in which Fn displays a highly extended conformation. The versatility of the AuTSNP as nano-biosensors and their applicability to the cellular environment presents them as a powerful new tool to signature in cell and potentially in vivo protein conformation and conformational transitions.

## Results and discussion

**LSPR sensing of Fn conformations.** The different conformations of Fn; compact at pH 8 and pH 7 and extended at pH 4 were verified by DLS measurements as shown in Figure 1b). The DLS hydrodynamic diameter values for compact Fn of 23 ± 3 nm are in agreement with literature values.[13]

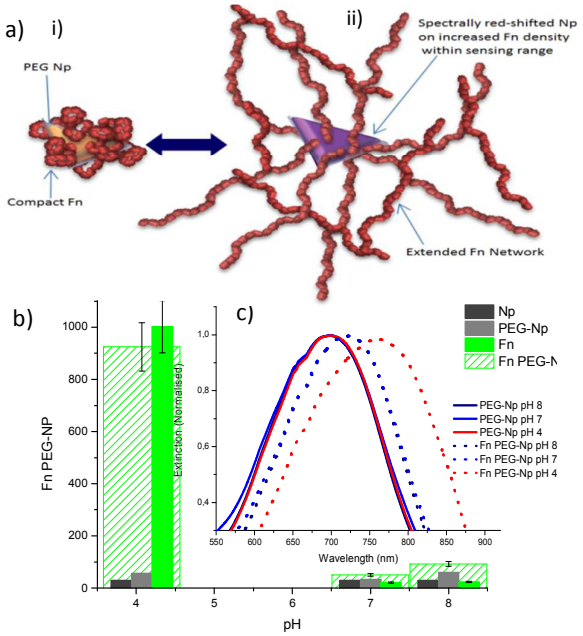


**Figure 1.** a) Schematic showing PEG coated nanoplates in the presence of Fn, i) with a compact conformation such as at pH 7 and 8. ii) with extended, networked conformation such as at pH 4. b) Representative DLS hydrodynamic diameter measurements for Fn, Nanoplates (Np), PEG coated nanoplates (PEG-Np) and PEG-Np in the presence of Fn at pH 4, pH 7 and pH 8. c) UV-Vis spectra at pH 4, pH 7 and pH 8 of PEG-Np and PEG-Np in the presence of Fn.

Hydrodynamic diameter values at pH 4 can vary from 400 nm to 1200 nm which, given the reported length of an extended Fn strand is 130 nm, indicates a degree of strand cross over and networking. DLS values for the nanoplates are in agreement with previously measured hydrodynamic diameters with negligible variability across the pH range. Polyethylene glycol coating of the nanoplates (PEG-Np) increases their hydrodynamic diameters by approximately 30 nm for pH 8 and pH 4 with a slightly smaller increase generally observed at pH 7, which may indicate that PEG binds more tightly to the nanoplate surface at pH 7 than at pH 8 or pH 4. Typically the hydrodynamic diameter of the PEG-Np in the presence of Fn is the sum of the constituent components at pH 8 and pH 7. Due to the networking of the extended Fn strands at pH 4 and the possible perturbation of the network by the presence of PEG-Np, hydrodynamic diameter values are generally reduced by approximately 5 % to 10 % compared to the Fn without PEG-Np. The overall minimal influence of the PEG-Np on the Fn hydrodynamic diameters is an important factor for non-disruptive LSRP sensing of Fn conformational changes. UV-vis spectra of PEG-Np and Fn incubated PEG-Np at each pH are shown in Figure 1c). The LSPR spectral position of the PEG-Np remains constant at pH 8, pH 7 and pH 4 confirming that the

PEG-Np remain largely unaltered within this pH range. The slight broadening of the pH 7 spectrum compared to those at pH 8 and pH 4 may be indicative of the variation in PEG surface binding at pH 7. On incubating the PEG-Np with Fn at each pH, significant shifts in the LSPR spectra are observed due to the presence of the higher refractive index Fn protein at the surface. The LSPR spectra for Fn incubated PEG-Np at pH 7 and pH 8 are red shifted by 18 nm and correspond to the presence of compact Fn at the PEG-Np surface. Again a slight broadening of the pH 7 Fn incubated PEG-Np spectrum compared to that of pH 8 is noted which may be associated with the PEG coated layer. Attachment or location of a compact Fn strand at a PEG-Np surface will occupy a larger surface area, but protrude less from the surface than an extended Fn strand network as depicted schematically in Figure 1a.

At pH 4, Fn incubated PEG-Np spectra are red shifted by as much as 60 nm indicating a larger density of Fn within the sensing range of the PEG-Np, than in the case of pH 8 and pH 7. The extent of these red shifts indicate that Fn in its compact form, folded about the nanoplate surface does not fill the sensing range of the PEG-Np and that PEG-Np LSPR continue to exhibit a spectral sensitivity response at length scales relevant to the extended Fn strands. The high aspect ratio of the nanoplates which increases the evanescent electric field decay length at the surface, facilitate this important feature which can enable pronounced LSPR spectral shifts in response to protein conformational activity spanning a scale of several tens of nm.

**LSPR sensing of Fn conformational changes**. Fn switching of conformations from compact to extended and extended to compact can be induced by pH adjustment. DLS measurements confirm Fn with a hydrodynamic diameter of 23 ± 3 nm at pH 8 unfolds to form an extended network with a hydrodynamic diameter in the range 400 nm to 1200 nm on the addition of citric acid bringing the pH to 4. On the addition of sodium phosphate buffer, pH 9, to Fn at pH 4, a size reduction to less than 30 nm is measured as the pH reaches 8. Corresponding hydrodynamic diameter changes were also observed for Fn upon pH adjustment in presence of PEG-Np.

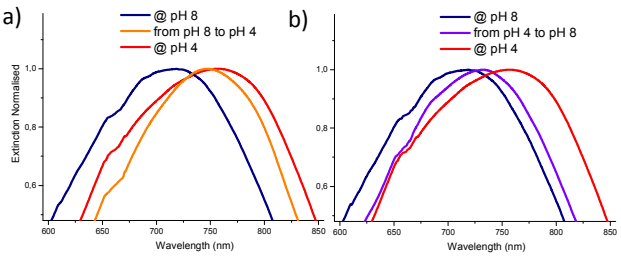


**Figure 2.** UV-Vis spectra of PEG-Np in the presence of Fn a) at pH 8 and pH 4 and on pH adjustment from pH 8 to pH 4 b) at pH 8 and pH 4 and on pH adjustment from pH 4 to pH 8.

UV-vis measurements of pH adjusted Fn incubated PEG-Np, (Figure 2a and 2b) were found to follow the DLS size trends, denoting Fn translation from contracted to extended conformation and extended to contracted conformation. Fn incubated PEG-Np at pH 8 were found to exhibit a significant 27 nm redshift on adjustment of the solution pH to 4. LSPR detection of Fn folding was also demonstrated where a significant 25 nm blue shift was observed on the adjustment of Fn incubated PEG-Np from pH 4 to pH 8. The large spectral shifts observed, the strong spectral differentiation between compact and extended Fn and the clear identification of changes in Fn conformation from folded to unfolded, highlight the capacity of the nanoplate LSPR sensing for in situ protein conformation detection. The red and blue shifts observed for the confor-mational changes induced by adjustment of the pH do not completely reach the original spectral positions measured for Fn incubated PEG-Np at pH 4 and pH 8, falling short by typically 10 nm. Steric hindrance effects such as the different numbers of Fn molecules which attach at pH 8 and pH 4, given the respectively larger and smaller areas occupied at the nanoplate surface by the contracted and expanded conformations, can contribute to the reduction in the spectral shifts. Upon unfolding (when the pH is adjusted from pH 8 to pH 4), space is created, enabling further extended Fn strands to interact close to the nanoplate surface, contributing to the spectral red shift. Steric hindrance due to the original attached Fn can, however, reduce the amount of Fn in the vicinity of the surface compared to initial incubation at pH 4, decreasing the extent of the red shift produced. DLS size measurements indicate that by increasing the pH to 8, the network of crossed Fn strands is broken up, resulting in a reduced number of Fn molecules close to the nanoplate surface, contributing to the observed blue shift. The folding of the larger numbers of Fn molecules attached to the surface can increase the amount of Fn within the nanoplate sensing range compared to initial incubation at pH 8, lessening the extent of the blue shift response.

**LSPR sensing of Fn cleavage with cathepsin.** Fn degradation by cathepsins including cathepsin B (CTSB) is an important cellular function and CTSB is an increasingly important human disease marker.23-25 Here LSPR spectral differentiation between Fn and CTSB digested Fn (Figure 3 a), where Fn was pre-treated with CTSB and subsequently incubated with PEG-Np, shows a distinctly blue shifted spectrum compared with incubation of PEG-Np with untreated Fn.

The shorter strands of the CSTB treated Fn reduce the density of the protein within the nanoplate sensing range, inducing a 31 nm blue shift in the LSPR spectral location. Furthermore, the treatment of Fn incubated PEG-Np with CTSB (Figure 3 b)), results in the real-time blue shifting of the LSPR spectrum, as cleavage of the Fn strands reduces the quantity of protein at the nanoplate surface, decreasing the local refractive index density. After 30 min CTSB incubation a 10 nm blue spectral shift is observed with a further 6 nm blue spectral shift observed after 120 min showing the real-time progression of the CSTB Fn digestion.

**LSPR serum assay for Fn Cleavage.** Given the prevalence of increased CTSB levels in diseases such as cancer, a simple assay for straight forward detection would provide a highly

useful diagnostic tool. Here, a versatile no-wash assay for the cleavage of Fn by CTSB in serum is demonstrated. Serum was added to Fn-incubated PEG-Np and allowed to incubate overnight to ensure the spectral shift response to the serum proteins, protein corona formation and non-specific binding interactions were complete. EDTA was added and the sample was divided into two aliquots with CTSB added to one of the aliquots.

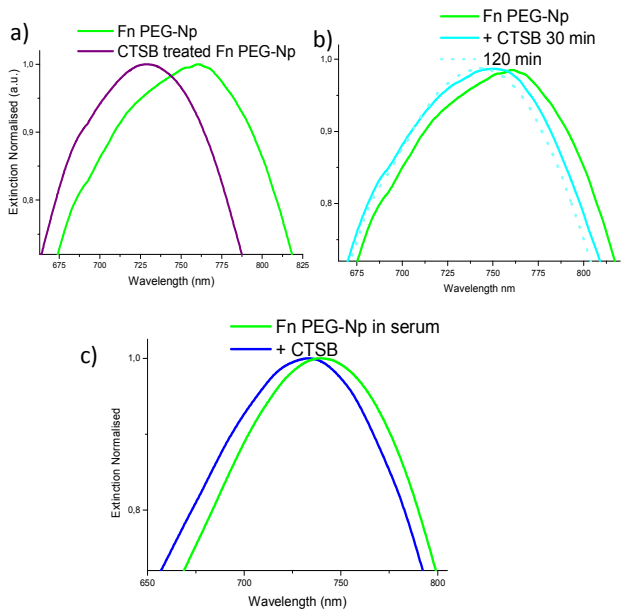


**Figure 3.** UV-Vis spectra of a) PEG-Np in the presence of Fn and PEG-Np in the presence of Fn treated with CTSB. b) PEG-Np in the presence of Fn with and without the addition of CTSB. c) Serum assay for CSTB cleavage of Fn, with and without the presence of CTSB

The measured spectral peak position of 747 nm for Fn PEG-Np incubated under the conditions for CTSB activity in serum at pH 4, shown in Figure 3, is 10 nm blue shifted compared with pH 4 buffer conditions measured in Figure 1c indicating somewhat reduced extension of the Fn. The blue shift also indicates the absence of any significant non-specific binding due to the serum proteins, providing evidence that Fn acts a strong inhibitor of non-specific binding enabling detection of the selective CTSB activity.

UV-vis spectra taken after incubation for 1 hour show a clear blue shift of 6 nm for the sample with CTSB compared to the control solution. This assay demon-strates the capability of the nanoplate LSPR to provide highly sensitive detection of changes to proteins attached to their surface within the complex serum environment. This assay can be readily optimised to provide a straight-forward no-wash assay method for the detection of disease related protein geometric and conformational changes in clinically relevant samples.

**LSPR sensing of Fn conformational changes in cell culture.** Demonstration of the detection of pro-ein conformational changes within the serum environ-ment highlights the potential of the nanoplates to provide clear spectral signalling of protein conformational changes occurring within the high background cellular environment.

Fn incubated with cells has been shown using FRET experiments to uncoil from its compact format at physiological pH to proceed to from extensive fibrils within the cellular environment.[32] Fn without nanoplates, PEG-Np and PEG-Np exposed to equivalent amounts of Fn and BSA were incubated with MDCK II cells for up to 72 hours. PEG-Np and BSA PEG-Np MDCK II cell incubations provide control experiments to monitor nanoplate protein corona formation, non-specific binding and influence on cellular morphology.[33-36] Fn without nanoplate MDCK II cell incubations provide control experiments to monitor the influence of Fn on cell morphology. The healthy morphological profile of each of the MDCKII cell samples, (Figure 4b i) to v)), indicates negligible adverse effects due to the presence of the nanoplates, Fn and BSA. UV-vis spectra of the Fn PEG-Np, (Figure 4a), exhibit extensive spectral red shifts over time with an extremely large 156 nm red shift recorded after 48 hours incubation. The strong spectral signal of the Fn PEG-Np over this time period is highly indicative of an LSPR response induced by the activity of the Fn conformational translation from compact to extended to form cellular fibril networks producing large volumes of high density refractive index protein regions within the vicinity of the nanoplate surfaces. These results support the model of Fn fibril assembly in which cellular integrins cause Fn extension, expose self-assembly sites which lead to Fn polymerization and the formation of fibrils which to grow longer and thicker dimensions over time.[37,38] Maturation of the ECM involves increased Fn unfolding and fibril formation and is associated with the majority contribution to the measured spectral response. Interactions such as cellular integrin binding to Fn domains and other secondary processes facilitating in the progression of Fn, contribute in part to the spectral response.[13,38] The very large Fn PEG-Np spectral shifts observed over time correlate well with models pos-tulating Fn as a marker for ECM aging[38] and demonstrate the strong capability of the nanoplates to provide continuous high sensitive recordings of Fn conformational activity within the cellular environment. Brightfield and fluorescent images of the actin stained MDCKII cells shown in figure 4b) are used to analyse the influence of Fn and nanoplates on the cells. Normal epithelial morphology is observed for MDCKII cells with and without the presence of nanoplates or Fn. The presence of PEG-Np and BSA PEG-Np (Figure 4b ii) and iii)) show an increased clustering of the cells (circle inset in fluorescent image in figure 4b ii) compared to the cells without nanoplates or Fn (Figure 4b i)). Additionally the top surface of the cellular layer is observed to exhibit increased undulations in the presence of PEG-Np and BSA PEG-Np. This undulating and wavy appearance of the surface is also observed in the case of Fn PEG-Np and to a lesser extent for Fn without the presence of nanoplates (Figure 4b iv) and v)) with a large number of clustered cells also visible. An assessment of several images of each of the samples shows cell organisation into

clusters typically covers approximately 5 % of the cell surface area in the case of MDCKII cells without the presence of nanoplates or Fn.

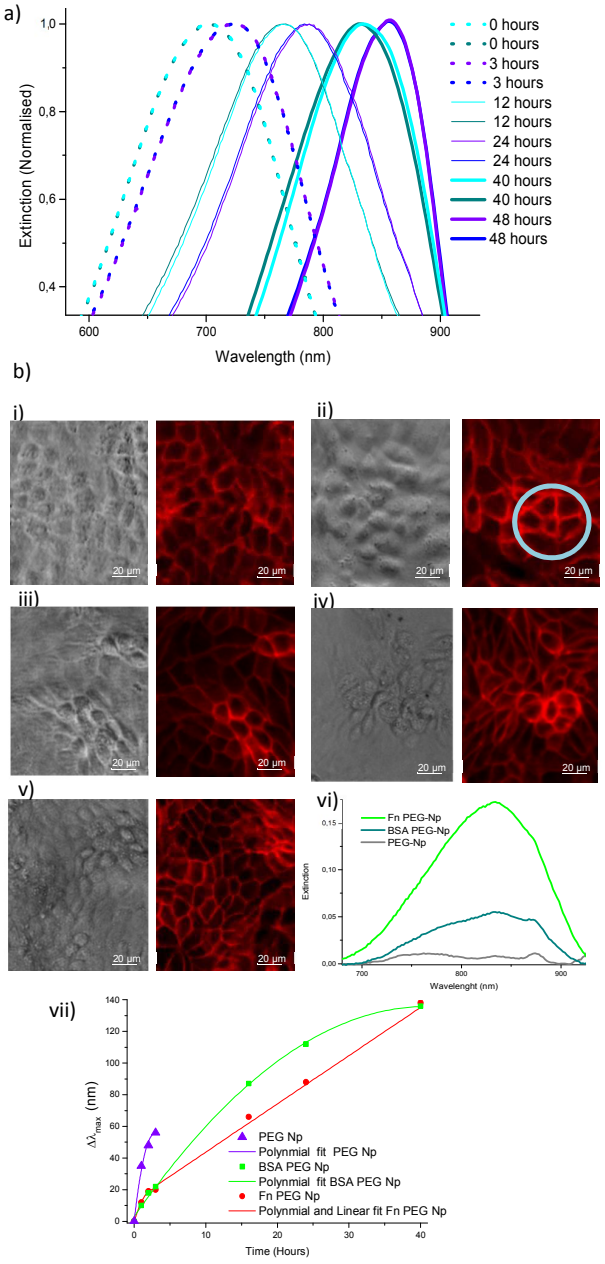


Figure 4. a) Duplicate UV-Vis spectra of Fn incubated PEG-Np in the presence of MDCK II cells over time from 0 hours to 48 hours. b) Brightfield and fluorescence images of actin stained MDCK II cells incubated for 72 hours with i) No nanoplates, ii) PEG-Np, iii) BSA PEG-Np, iv) Fn PEG-Np, v) Fn without nanoplates. Circle on fluorescent image ii) indicates a cluster of reorganised cells. vi) corresponding un-treated UV-Vis spectra for Fn PEG-Np, BSA-PEG Np and PEG-Np at 40 hours. vii) LSPR spectral shift of PEG-Np (violet), BSA PEG-Np (green), Fn PEG-Np (red) in the presence of MDCK II

Cell cluster coverage increases to approximately 15 % to 20 % for PEG-Np and BSA PEG-Np with a further increase to 70 % to 80 % coverage for Fn PEG-Np and Fn without the presence of nanoplates. The high cell reorganisation levels for Fn PEG-Np and Fn without the presence of nanoplates is evidence of Fn alteration of the native extracellular matrix due to Fn fibril formation. These observations are in agreement with reports that cells actively change Fn conformation within an evolving ECM. Increased ECM rigidity is found as cells increasingly unfold, stretch and align Fn over time scales of up to 72 hours.[38]

The morphological changes observed in Figure 4b) iv) and v) can be associated with this physical alteration of the ECM. Fn extension and unfolding within the ECM is associated with known cellular actin responses including actin polymerization and cytoskeletal stiffening due to alignment of force-bearing actin stress fibers.[38] In our experiments, enhanced alignment of fibronectin fibrils as well as actin fibers observed over time, are indicative of increased tension and stiffening of the ECM as it matures. Increased actin localization is visible at cellular borders, which can be associated with the formation of adhesion foci within the cellular clusters.

Nanoparticles are typically up-taken by cells.[39] Distinctive differences are found between un-smoothed and un-normalised UV-Vis spectra of PEG-Np, BSA PEG-Np and Fn PEG-Np measured after 40 hours of incubation with MDCK II cells, shown in Figure 4 b vi). These differences correspond to the localisation within the cellular environment and the degree of resistance to cellular degradation. The LSPR spectral profile for the PEG-Np cannot be distinguished indicating that these nanoplates, which do not have a protective protein covering, have been disintegrated by the cellular conditions (see Figure S3). The BSA PEG-Np show a much reduced spectral intensity compared with the Fn PEG-Np indicating a significant degree of degradation due to the cellular conditions. The broadness of the BSA PEG-Np spectrum, the deterioration of the characteristic LSPR spectral profile and its strongly red shifted location indicate a degree of nanoplate degradation and non-specific binding of cellular proteins and cellular constituents. In contrast the Fn PEG-Np retain their characteristic LSPR spectral profile after extensive red spectral shifts over the 40 hour period which indicates that degradation due to the cellular environment and non-specific binding are not the primary factors responsible for this spectral signature. The high salinity of physiological environments will degrade and dissolve non-protected silver nanoparticles. Gold edge coating and surface protein attachment can provide protection, however, within cellular environment, complex cellular activity results in the degradation of the nanoplates. The incorporation of the Fn PEG-Np within the ECM offers further protection in addition to protective coatings from the cellular degradation processes extending the duration of their intact spectra profile. Nonetheless, Fn PEG-Np will also be subject to cellular activity, in particular Fn degra-dation mechanisms.

This differentiation between the PEG-Np, BSA-Np and Fn PEG-Np is emphasized by the profile of the spectral peak shift over time shown in Figure 4b vi). PEG-Np, which lacks the presence of surface protein protection shows an increased spectral shift rate with disintegration of the spectral profile past the 3 hour time point. This can be associated with non-specific binding,

degradation, cellular uptake and digestion of the PEG-Nps. Non-specific bind is found to follow a nonlinear spectral shift profile (Figure S1) for nanoplates in the presence of cells and cell free media (Figure 4 b vi) and Figure S1. A significant difference is noted for the Fn PEG-Np which exhibits a linear red shift response in contrast to the nonlinear red shift profile of PEG-NP, BSA PEG-NP in the presence of MDCK II cells. The Fn PEG-Np spectral shift response in fact appears to follow a nonlinear trend up to the 3 hour time point as shown in Figure S2a followed by distinct transition to a linear progression. The work of Vogel et al has shown that on adding Fn added to cells observation of Fn matrix fabrication takes up to 4 hours to occur.[36-38] There is a strong correlation between this time and the transition from nonlinear to linear progression of the spectral shift rate of Fn PEG-Np incubated with MDCK II (Figure 4b vi), Figure S2a and S2b). These results provide evidence that from the 3 hour time point the Fn PEG-Np have been actively integrated into the ECM and the Fn associated with the Fn PEG-Np is undergoing incorporation, via the reported route of cellular integrin binding induced Fn uncoiling, extension and assimilation into Fn fibril networks. Further evidence that the Fn PEG-Np spectral response in the presence of MDCK II cells is due to Fn conformational activity, is given by the fact that the overall Fn PEG-Np spectral shift is larger than that of BSA PEG-Np despite the fact that Fn PEG-Np having demonstrated strongly reduced non-specific binding compared to BSA PEG-Np in cell free media as seen in Figure S1 and the absence of observed non-specific binding in the serum assay.

The demonstrated capacity to exhibit large spectral shifts over periods of days in response to the progression of ECM protein conformational transition events underlines the strong potential of the nanoplates for the versatile and straight forward detection and monitoring of protein conformational behaviour within cellular environments.

## Experimental

**Reagents and Materials:** Reagents were ob-tained from Sigma-Aldrich and used as received. Epithelial Madin Darby Canine kidney (MDCK II) cells were kindly donated by Dr, Frédéric Luton, Institute of Cellular and Molecular Pharmacology, Valbonne, France.

**Instrumentation:** UV-vis extinction measure-ments were performed with unpolarized white light coupled to a portable fiberoptic spectrometer (Ocean Optic USB4000) using 1 cm path length micovolume cuvettes in standard transmission geometry. The real time response was recorded using 70 ms integration time without averaging and smoothed using a ST averaging function. UV-vis extinction measurements on cells were performed using a plate-reader spectrometer (Tecan). Dynamic light scattering (DLS) measurements were performed on a Malvern Nanosizer-S. The immunofluorescence samples were examined with an epifluorescent microscope (Axio Observer Z1, Carl Zeiss).

**Au-edge-coated TSNP (Nanoplate) synthesis:** Triangular Silver Nanoplate (TSNP) sols were prepared using the silver seed-catalyzed reduction of $AgNO_3$ as previously described.[27,28,40]. The process involves combining 5 mL distilled water, aqueous ascorbic acid (75 µL, 10 mM) and various quantities of seed solution, followed by addition of 3 mL aqueous $AgNO_3$ (0.5 mM) at a rate of 1 mL min-1.Au-edge-coated TSNP were synthesized from TSNPs prepared using a previously report[27] method.[23] A thin coating of gold was applied onto the edges of the nanoplates by adding 150 µL of 10 mM ascorbic acid to the TSNP solution and adding an appropriate volume of chloroauric acid ($HAuCl_4$) with a syringe pump at a rate of 0.2 mL.min-1, while stirring the solution. The AuTSNP used here have a LSPR peak wavelength at 694 nm, are 40 ± 4 nm in size, have an aspect ratio of 7 ± 0.5 and a LSRP refractive index sensitivity of 420 nm/RIU.[27,28] The AuTSNP were coated with 0.01% (Mw 16,000 – 24,000), polyethylene glycol (PEG-Np), which red shifts their LSPR by 8 nm. The PEG serves to minimise the influence of Fn direct contact with the nanoplate surface on its conforma-tional behaviour.

LSPR sensing of pH induced Fn conforma-tional changes. Solution samples of pH induced Fn conformational configurations and pH adjusted conformational changes were prepared in order to examine the capability of the nanoplate LSPR to detect and monitor these events. A sodium phosphate buffer system with NaCl was selected in order to facilitate a wide pH range. Fn aliquots were pre-exposed for at least 30 min. to a given pH in order to establish their characteristic conformations. Typically 25 µL of 0.1mg/ml Fn was incubated with 350 µL of 0.01 M $Na_2HPO_4$, 0.01 M NaCl at room temperature. Upon verification of the Fn size and conformation using DLS, 50 µL of PEG-Np was added to each sample and incubated at room temperature. DLS measurements were used to monitor the size of the Fn PEG-Np complexes. UV-vis measurements of the nanoplate LSPR spectral response were carried out.

In order to demonstrate LSPR measurements of changes in Fn conformations, the pH of the solutions was adjusted from pH 4 to 8 by adding 160 µL 0.1 M $Na_2HPO_4$ pH 9 and from pH 8 to 4 by adding 30 µL of 55 mM citric acid. Samples of Fn with and without the presence of nanoplates were incubated at room temperature and tested using both DLS and UV-Vis measurements.

**LSPR sensing of Fn Cleavage with Cathepsin.** A series of experiments were carried out in order to examine the The immunofluorescence samples were examined with an epifluorescent microscope (Axio Observer Z1, Carl Zeiss). 20 µl of 40 mM EDTA was added to 50 µL of pre-incubated 0.1mg/ml Fn in PBS. When using nanoplates 100 µL of PEG-Np were added and PB added bringing the total volume to 400 µL. DLS and UV-Vis measurements were used to determine the results.

LSPR serum assay for Fn Cleavage: A straightforward wash-free LSPR test for the detection of Fn cleavage by CTSB in serum was carried out using UV-Vis spectroscopy. Fn (50 µL, 0.01 mg/ml) and 100 µL PEG-Np were pre-incubated for 1 hour in 400 µL 0.01 M $NaPHO_4$, 0.01 M NaCl, pH 4 until LSPR spectral shift remained constant. 10 µL undiluted fetal bovine serum was added and incubated overnight. 20 µL of 40 mM EDTA was added and the sample was then divided into 2 aliquots. CTSB (25 µL of 0.01mg/ml) was added to one aliquot and both

samples were incubated at room temp. UV-Vis measurement and were taken immediately and after 1 hour.

**LSPR sensing of Fn conformational changes in cell culture:** Fn incubated nanoplates were added to MDCK II cells and monitored over 24 hours using UV-Vis spectroscopy in order to determine the potential of the nanoplate LSPR to indicate and observe Fn conformational changes within the presence of cells and in particular to observe the process of Fn unfolding and formation of fibrils, MDCK II cells were routinely maintained at 37°C in a humidified atmosphere of 5% CO2 in complete DMEM (cDMEM) media (Dulbecco's Modified Eagle Medium, 10% fetal bovine serum, and Pen/Strep 5000 [U/mL] penicillin–5000 [µg/mL] streptomycin). For all experiments, cells were plated at an initial density of 2 x $10^5$ cells/$cm^2$ in 96 well plates and incubated until confluence was reached. Prior to commencing the experiments, the media was changed to phenol red-free cDMEM to avoid interference with the spectroscopic measurements. Nanoplates and protein exposed nanoplates were incubated with MDCKII cell cultures (a nanoplates-phenol red-free cDMEM ratio of 1:1) and incubated at 37°C and 5% $CO_2$ for indicated times.

Specifically, 300 µL of nanoplates and 10 µL of 1 mg/ml Fn were pre incubated and added to the cells. Equivalently 300 µL of nanoplates and 10 µL of 1 mg/ml BSA were pre incubated and added to the cells as a con-trol. 10 µL of 1 mg/ml Fn without the presence of nano-plates was also added to the cells as a further control.

**Actin fluorescence staining to examine cells morphological changes and reorganization:** Cells were washed three times with cold PBS+ ( PBS pH 7.4 with 10 mM $CaCl_2$ and 5 mM $MgCl_2$), and subsequently fixed with 4% paraformaldehyde in PBS+ for 30 min at 4° C. After 3 quick rinses, the cells were incubated in quenching solution (1 M glycine, 1 M (NH4)2SO4 in PBS+) during 10 min at room temperature. Three rinses with PBS+ were performed. For permeabilization and blocking steps, the cells were incubated with PFS solution (PBS+ with 0.025% saponin and 0.7% fish skin gelatin) for 30 min at 4°C. Actin was stained with Rhodamine Phallotoxin (Invitrogen) diluted 1:2000 in PFS solution. After rinsing, the monolayers were examined under the fluorescent microscope (Axio Observer Z1, Carl Zeiss).

## Conclusions

Conformational transitions of the ubiquitous protein fibronectin, were detected using solution phase nano-plates which exhibit some of the highest refractive index sensitivity values recorded to date both in solution and for the first time within the presence of living cells. Using the LSPR spectral shifts, a 38 nm red shift distinguishes between pH induced compact and extended Fn conformations. A strong red shift of 27 nm accompanies the conformational transition of Fn from compact to extended while a corresponding blue spectral shift of 25 nm accompanies the transition from extended to compact conformation. The spectral shifts observed are associated with changes in the density of the refractive index within the vicinity of the nanoplate surface due to the Fn conformational transitions.

Digestion of Fn by CTSB is associated with blue spectral shifts corresponding to a reduction in the protein density and therefore refractive index local to the nanoplate surface as the size of the Fn is reduced. A straightforward no-wash assay for the serum detection of Fn digestion by CTSB is demonstrated which can readily be optimised with potential for use within the clinical settings for the disease assessment such as cancer metastasis. The progression of Fn diffusely bound to cells in a compact state to form Fn fibril matrices in which Fn displays a highly extended conformation generated very large LSPR spectral shifts of 156 nm over 48 hours and was accompanied by morphological re-arrangement of the MDCK II cells. These results correlate with the Fn model in which Fn continuously unfolds and extends within cells, binding to form fibrils which grow and become thicker in an evolving ECM. The versatility and label-free feature of the nanoplates and in particular their capability to detect and monitor protein structural and conformational transitions in cellular environments presents them as a powerful new tool to signature protein conformational activity in living cells.

## Acknowledgements

The research leading to these results has received funding from the European Commission's Seventh Framework Programmes Marie Curie IEF, 328466 ProtEProbe.

## Notes and references

1 M. Ramirez-Alvarado, J. W. Kelly and C. M. Dobson, Protein Misfolding Diseases: Current and Emerging Principles and Therapies, John Wiley & Sons, 2010.
2 N. F. Bence, R. M. Sampat and R. R Kopito, *Science,* 2001, **292**, 1552.
3 Y. C. Tsai and A. M. Weissman, *Genes & Cancer* 2010, 1, 764.
4 M. R. Buck, D. G. Karustis, N. A. Day, K. V. Honn and B. F. Sloane, *Biochem. J.*, 1992, **282**, 273.
5 J. T. Pelton and L. R. McLean, L. R. *Anal. Biochem*. 2000, **277,** 167
6 R. Ishima, R. and D. A. Torchia, *Nat. Struct. Biol*. 2000, **7**, 740.
7 S. Ebbinghaus and M. Gruebele, *J. Phys. Chem. Lett.* 2011, **2,** 314.
8 S. Ghaemmaghami, and T.G. Oas, T. G. *Nat. Struct. Biol*. 2001, **8**, 879
9 L. M. Charlton and G. J. Pielak, *Proc. Natl. Acad. Sci. U.S.A*. 2006, **103**, 11817
10 K. Truong, and M. Ikura, M. *Curr. Opin. Struct. Biol.* 2001, **11**, 573.
11 T. Heyduk, *Curr. Opin. Biotechnol*. 2002, *13*, 292.
12 D. Axelrod, D. *Traffic*, 2001, **2,** 764
13 N. M. Tooney, M. W. Mosesson, D. L. Amrani, J. F Hainfeld and J. S. and Wall. *J. Cell Bio.* 97, 1686
14 M. L. Smith, D. Gourdon, W. C. Little, K. E. Kubow, R. A. Eguiluz, S. Luna-Morris, V. Vogel *PLoS Biol.* 2007, 5, e268.
**15** P. Singh, C. Carraher, and J. E. Schwarzbauer, *Annu Rev Cell Dev Biol*. 2010, **26**, 397**.**
16 X. Yang, H. Huang, Z. Zeng, L. Zhao, P. Hu, D. He, X. Tang, Z. Zeng, *Clin. Biochem.* 2013, **46**, 1377.
17 S. Midwood, L. V. Williams and J.E. Schwarzbauer, *Int. J. Biochem. Cell Biol.*, 2004 **36**, 1031.

18 M. P. Welch, G.F Odland and R. A. Clark *J. Cell Biol*., 1990, **110**, 133.
19 M. D. Wan, E. M. Chandler, M, Madhavan, D. W. Infanger, C. K. Ober, D. Gourdon, G. G. Malliaras, C. Fischbach, *Biochimica et Biophysica Acta,* 2013, **1830**, 4314.
20 E. M. Chandler, M. P. Saunders, C. J. Yoon, D. Gourdon, C. Fischbach, *Phys. Biol*., 2011, **8**, 015008.
21 B. Werle B. Julke B, T. Lah, E. Spiess, and W. Ebert, *Brit. J Cancer*, 1997; **75**, 1137.
22 D. Kuester, H. Lippert, A. Roessner and S. Krueger, *Pathol. Res. Pract*., 2008, **204**, 491.
23 N. P. Withana, G. Blum, M. Sameni, C. Slaney, A. Anbalagan, M. B. Olive, B. N. Bidwell, L. Edgington, L. Wang, K. Moin, B. F. Sloane, Robin L. Anderson, M. S. Bogyo and B. S. Parker, *Cancer Res.,* 2012, **72**, 1199.
24 G. J. Tan, Z.K Peng, J. P. Lu, F. Q. Tang**,** *World J Biol Chem*, 2013, **4**, 91-101
25 H. Zhang, T. Fu, S. McGettigan, S. Kumar, S. Liu, D. Speicher, L. Schuchter, and X. Xu, *Int J Mol Sci*. 2011, **12**, 1505.
26 W. P. Hall, J. Modica, J. Anker, Y. Lin, M. Mrksich, and R. P. Van Duyne, *Nano Lett.* 2011, **11**, 1098
27 Y. Zhang, D. E. Charles, D. M. Ledwith, D. Aherne, S. Cunningham, M. Voisin, W.J. Blau, Y. K. Gun'ko, J. M. Kelly and M. E. Brennan-Fournet, *RSC Adv*., 2014, **4**, 29022.
28 D.E. Charles, D, Aherne, M. Gara, D. M.Ledwith, Y. K. Gun'ko, J. M. Kelly, W. J. Blau and M. E. Brennan-Fournet, *ACS Nano 2010*, 4, 55.
29 D.E Charles, M. Gara, D. Aherne, D. M. Ledwith, J. M. Kelly, W. J. Blau, and M. E. Brennan-Fournet, *Plasmonics*, 2011, **6**, 351.
30 G. Barbillion, G. *J. Mat. Sci. Eng.* 2010, **4**, 69.
31 A. J. Haes and R. P. Van Duyne, *Anal. and Bioanal. Chem.* 2004, **379**, 920
32 G. Baneyx, L. Baugh and V. Vogel, *PNAS*, 2001, 98, 14464.
33 B. D. Chithrani, A. A. Ghazani and W. C. Chan, *Nano Lett.* 2006, **6**, 662.
34 E. C. Cho, J. Xie, P. A. Wurm and Y. Xia Y. *Nano Lett.* 2009, **9**, 1080.
35 M. S. Ehrenberg, A. E. Friedman, J. N. Finkelstein, G. Oberdörster and J. L. McGrath, *Biomaterials.* 2009, **30**, 603.
36 N. Oh, J. Park, *Int. J. Nanomed*. 2014, **9**, 51.
37 J. E. Schwarzbauer and J. L. Sechler, *Curr. Opin. Cell Biol.* 1999. *11*, 622.
38 M. Antia, G. Baneyx, K. E. Kubow and V. Vogel, *Faraday Discuss*. 2008 ; 139: 229.
39 J. A. Yang, H. T. Phan, S. Vaidya S. and C. J. Murphy, *Nano Lett*., 2013, **13**, 2295.
40 D. Aherne, D. E. Charles, M. E. Brennan-Fournet, J. M. Kelly, J and Y. K. Gun'ko, *Langmuir,* 2009, **25**, 10165.

Nanoplates enable high sensitive spectral monitoring of fibronectin conformational transitions and fibril formation within the extra cellular matrix of live cells.

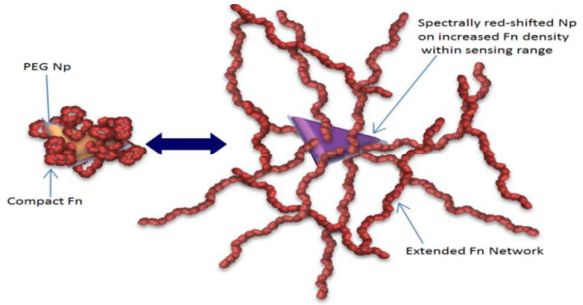


Np